

Size Information Obtained by Using Static Light Scattering Technique

Yong Sun

February 13, 2019

Abstract

Detailed investigation of static light scattering (*SLS*) has been attempted in this work based on dilute water dispersions of homogenous spherical particles, poly(*N*-isopropylacrylamide) microgels and simulative data. When Rayleigh-Gan-Debye approximation is valid, for the large particles, the simple size information, the static radius R_s and distribution $G(R_s)$, can be accurately obtained from SLS. Through the theoretical analysis, for the small particles, the root mean-square radius of gyration $\langle R_g^2 \rangle^{1/2}$ and the molecular mass of particles measured by using the Zimm plot are discussed. The results show that the molecular mass measured by using the Zimm plot over the average molecular mass of particles is a function of the size distribution.

1 Introduction

The intensity of the scattered light is determined by the sizes, shapes and interaction among the particles in the scattering medium. Developed during the last few decades, dynamic light scattering (*DLS*) is widely used to obtain the size information of particles for colloidal dispersion systems. Although the static light scattering (*SLS*) spectroscopy contains more sensitive size information, in general, the measurements of SLS spectroscopy are simplified to the Zimm plot, Berry plot or Guinier plot etc. to obtain the root mean-square radius of gyration $\langle R_g^2 \rangle^{1/2}$ and the molecular mass of particles provided that the particle sizes are small. Since it is hard to obtain the particle size distribution for small poly-disperse systems by using DLS technique, for dilute poly-disperse homogeneous spherical particles, Pusey and van Megen¹ proposed a method to detect small poly-dispersities when the Rayleigh-Gans-Debye (*RGD*) approximation is valid, by measuring the dependence of the effective diffusion coefficient obtained from the initial slope of the correlation function with respect to the scattering angle. By definition, the effective diffusion coefficient is the intensity-weighted average diffusion coefficient. Both theoretical and experimental results show that the angular dependence of the light scattering intensity is a sensitive function of the particle's size and distribution.

How to obtain the particle size distributions from the SLS data has been researched by a few authors. Hallett and Strawbridge² have studied the theoretical scattering intensity of a coated sphere with vertically polarized incident light. Then the scattered intensity at the geometrical or linear trial radii between r_{\min} and r_{\max} was used to fit the SLS data. Schnablegger and Glatter³ assumed that the size distribution can be described as a series of cubic B-splines, then used the simulative data and measured data to demonstrate the computation procedure.

In this article, we deal with the dilute poly-disperse homogeneous spherical particles. We assume that the number distribution of particles is Gaussian and we consider the effects of the form factor and the scattering intensity-weighted differences of different size particles on the light scattering intensity. Then with the assistance of a non-linear least squares fitting program (*NLLSQ*), the mean particle size \bar{R}_s and the standard deviation σ are obtained. With this treatment, we can avoid the constraints of the Zimm plot, Berry plot, Guinier plot etc. on measurement, and their stringent dependence on sample quality and instrument at small angles. For large particles, size distributions can be measured accurately. With the assistance of simulative data, the effects of the reflective light and noises have been investigated in detail. Through the theoretical and simulative data analysis, the root mean-square radius of gyration $\langle R_g^2 \rangle^{1/2}$ and the molecular mass of particles measured by using the Zimm plot are also discussed. The results show that the molecular mass measured by using the Zimm plot over the average molecular mass of particles is a function of the size distribution. With theoretical and experimental data analysis, better understanding of the size information contained in SLS spectroscopies is obtained.

2 Theory

For simplicity, we consider homogeneous spherical particles and assume that the RGD approximation is valid. The static light-scattering intensity of a dilute non-interacting polydisperse system in unit volume can be obtained for vertically polarized light

$$\frac{I_s}{I_{inc}} = \frac{4\pi^2 \sin^2 \theta_1 n_s^2 \left(\frac{dn}{dc} \right)_{c=0}^2 c}{\lambda^4 r^2} \frac{4\pi \rho}{3} \frac{\int_0^\infty R_s^6 P(q, R_s) G(R_s) dR_s}{\int_0^\infty R_s^3 G(R_s) dR_s} \quad (1)$$

where θ_1 is the angle between the polarization of the incident electric field and the propagation direction of the scattered field, c is the concentration of particles, r is the distance between the scattering particle and the point of the intensity measurement, ρ is the density of the particles, I_{inc} is the incident light intensity, I_s is the intensity of the scattered light that reaches the detector, $q = \frac{4\pi}{\lambda} n_s \sin \frac{\theta}{2}$ is the scattering vector, λ is the wavelength of the incident light in vacuo, n_s is the solvent refractive index, θ is the scattering angle, $P(q, R_s)$

is the form factor of homogeneous spherical particles

$$P(q, R_s) = \frac{9}{q^6 R_s^6} (\sin(qR_s) - qR_s \cos(qR_s))^2 \quad (2)$$

and $G(R_s)$ is the number distribution. In this paper, the number distribution is chosen as a Gaussian distribution

$$G(R_s; \bar{R}_s, \sigma) = \frac{1}{\sigma \sqrt{2\pi}} \exp\left(-\frac{1}{2} \left(\frac{R_s - \bar{R}_s}{\sigma}\right)^2\right), \quad (3)$$

where \bar{R}_s is the mean static radius and σ is the standard deviation relative to the mean static radius.

If the reflective light is considered, the static light-scattering intensity in unit volume is written as

$$\frac{I_s}{I_{inc}} = a \frac{4\pi\rho}{3} \frac{\int_0^\infty R_s^6 P(q, R_s) G(R_s) dR_s + b \int_0^\infty R_s^6 P(q', R_s) G(R_s) dR_s}{\int_0^\infty R_s^3 G(R_s) dR_s} \quad (4)$$

where

$$a = \frac{4\pi^2 \sin^2 \theta_1 n_s^2 \left(\frac{dn}{dc}\right)_{c=0}^2 c}{\lambda^4 r^2} \quad (5)$$

and

$$q' = \frac{4\pi}{\lambda} n_s \sin \frac{\pi - \theta}{2} \quad (6)$$

is the scattering vector of the reflective light. b is a constant decided by the shape of sample cell, the refractive indices of the solvent & the sample cell and the structure of instruments.

When the values of qR_s are small, the form factor can be expanded and Eq. 1 can be written as

$$\frac{4\pi^2 \sin^2 \theta_1 n_s^2 \left(\frac{dn}{dc}\right)_{c=0}^2 c}{\lambda^4 r^2 N_0 \frac{I_s}{I_{inc}}} = \frac{\left(\int_0^\infty R_s^3 G(R_s) dR_s\right)^2}{\langle M \rangle \int_0^\infty R_s^6 G(R_s) dR_s} \left(1 + \frac{q^2 \int_0^\infty R_s^8 G(R_s) dR_s}{5 \int_0^\infty R_s^6 G(R_s) dR_s} + \dots\right) \quad (7)$$

where N_0 is the Avogadro's number, $\langle M \rangle$ is the average molecular mass of particles. It is defined as

$$\langle M \rangle = \frac{4\pi\rho N_0}{3} \int_0^\infty R_s^3 G(R_s) dR_s. \quad (8)$$

Comparing with the Zimm plot analysis⁴⁻⁶, the mean square radius of gyration, $\langle R_g^2 \rangle$, for a polydisperse system is

$$\langle R_g^2 \rangle = \frac{3 \int_0^\infty R_s^8 G(R_s) dR_s}{5 \int_0^\infty R_s^6 G(R_s) dR_s} \quad (9)$$

and the molecular mass of particles measured by using the Zimm plot is

$$M_z = \frac{\langle M \rangle \int_0^\infty R_s^6 G(R_s) dR_s}{(\int_0^\infty R_s^3 G(R_s) dR_s)^2}. \quad (10)$$

3 Experiment

The SLS spectroscopies were measured by using the instrument built by ALV-Laser Vertriebsgesellschaft m.b.H (Langen, Germany). It utilizes an ALV-5000 Multiple Tau Digital Correlator and a JDS Uniphase 1145P He-Ne laser to provide a 23 mW vertically polarized laser at wavelength 632.8 nm.

In this experiment, *N*-isopropylacrylamide (NIPAM, monomer) from Acros Organics was recrystallized from hexane/acetone solution. Potassium persulfate (KPS, initiator) and *N,N'*-methylenebisacrylamide (BIS, cross-linker) from Aldrich were used as received. Fresh de-ionized water from a Milli-Q Plus water purification system (Millipore, Bedford, with a 0.2 μm filter) was used throughout the whole experiment. The synthesis of gel particles was described elsewhere^{7,8} and the recipes of the batches used in this work are listed in Table 1.

Table 1. Synthesis conditions for NIPAM particles.

Sample	T ($^{\circ}\text{C}$)	t (hrs)	$W_N + W_B$ (g)	KPS (mg)	n_B/n_N
<i>PNIPAM</i> – 0	70 ± 1	4.0	1.00	40	0
<i>PNIPAM</i> – 1	70 ± 1	4.0	1.00	40	1.0%
<i>PNIPAM</i> – 2	70 ± 1	4.0	1.00	40	2.0%
<i>PNIPAM</i> – 5	70 ± 1	4.0	1.00	40	5.0%

The four samples were centrifugated four times respectively at 14,500 RPM, each followed by decantation of the supernatants to remove of free ions and any possible linear chains and disperse again in fresh de-ionized water. Then the no added cross-linker sample *PNIPAM* – 0 was diluted to $5.9 * 10^{-6}$, the sample *PNIPAM* – 1 that the molar ratio of *N,N'*-methylenebisacrylamide over *N*-isopropylacrylamide is 1% to $8.56 * 10^{-6}$, the sample *PNIPAM* – 2 that the molar ratio is 2% to $9.99 * 10^{-6}$ and the sample *PNIPAM* – 5 that the molar ratio is 5% to $8.38 * 10^{-6}$. Before the measurements were made, 0.45 μm filters (Millipore, Bedford) were used to do dust free for the samples *PNIPAM* – 1, *PNIPAM* – 2 and *PNIPAM* – 5.

4 Data Analysis

How to obtain the size information from SLS is shown in this section. The experimental data of the *PNIPAM* microgel samples was used to show the fitting process and the simulative data was used to check the effects of the different reflective light and the noises on the fitted results and the effects of the distribution on the molecular mass of particles measured by using the Zimm plot.

4.1 Experimental Data Analysis

When Eq. 1 was used to fit the $\frac{I_s}{I_{inc}}$ vs q data of the sample *PNIPAM* – 1 measured at temperature $29^\circ C$, the fitted mean radii \bar{R}_s and the standard deviations σ at different scattering vector ranges are listed in Table 4.1. The results show that the fitted result's errors decrease and the mean radius and the standard deviation approximate constant values when the fitting scattering vector range is enlarged. If the fitting scattering vector range continues to increase, the values of the radius and standard deviation begin to change and χ^2 changes to big. This is the results of the deviation between the real and the theoretical light scattering intensity in the vicinity of the $\frac{I_s}{I_{inc}}$'s minimum. This minimum lies at about the scattering vector 0.0177 nm^{-1} . In this range, most of the scattering light is cancelled due to the light interference. So many other characters of the particles can show the effect on the light scattering intensity, for example: the number distribution deviates from the Gaussian distribution, the particle shape deviates from a perfect sphere, the density of particles deviates from the homogenous density and the light scattering intensity from the solvent, etc. In order to avoid the effect of light interference, the fitted results during the scattering vector range 0.00345 nm^{-1} to 0.01517 nm^{-1} are chosen as the size information obtained by using the SLS technique. In order to check the effects of the different fitting ranges of the scattering vector, the experimental data was fitted again by fixing the larger value of q and decreasing the fitting range. The fitted results also are shown in Table 4.1. The values show the fitted results approximate constant values when the fitting range has enough large. Figure 4.1 shows the fitted result and the residuals during the scattering vector range 0.00345 nm^{-1} to 0.01517 nm^{-1} .

Table 4.1 The fitted results of the sample *PNIPAM* – 1 at different scattering vector ranges and $T=29^\circ C$.

$q (10^{-3} \text{ nm}^{-1})$	$\bar{R}_s (\text{nm})$	$\sigma (\text{nm})$	χ^2
3.45 to 9.05	260.09 ± 9.81	12.66 ± 19.81	1.64
3.45 to 11.18	260.30 ± 1.49	12.30 ± 3.37	1.65
3.45 to 13.23	253.45 ± 0.69	22.80 ± 0.94	2.26
3.45 to 14.21	254.10 ± 0.15	21.94 ± 0.36	2.03
3.45 to 15.17	254.34 ± 0.12	21.47 ± 0.33	2.15
3.45 to 17.00	255.40 ± 0.10	17.32 ± 0.22	11.02
5.50 to 15.17	254.24 ± 0.15	21.95 ± 0.47	2.32
7.95 to 15.17	254.32 ± 0.16	21.56 ± 0.57	2.38
10.12 to 15.17	254.65 ± 0.10	17.81 ± 0.63	0.79
12.21 to 15.17	254.84 ± 0.16	19.33 ± 0.87	0.42

If the reflective light was considered, Eq. 4 was used to fit all data in the whole scattering vector range. The fitted results are listed in Table 4.2. From the fitted results, the values of χ^2 are too big, the value of mean static radius \bar{R}_s is equal to that obtained by using Eq. 1 in the fitting range with the small values of the scattering vector and the standard deviation changes to small.

Table 4.2 The fitted results of the sample *PNIPAM*–1 were obtained by using Eq. 4.

b	$R_s(nm)$	$\sigma(nm)$	χ^2
0.01	254.0 ± 0.3	14.4 ± 0.5	194.60
0.011	254.0 ± 0.3	14.6 ± 0.5	168.20
0.012	254.0 ± 0.3	14.7 ± 0.5	149.99
0.013	254.0 ± 0.2	14.8 ± 0.4	139.82
0.014	254.1 ± 0.2	15.0 ± 0.4	137.52
0.015	254.1 ± 0.2	15.1 ± 0.4	142.96
0.016	254.09 ± 0.07	15.2 ± 0.5	155.97
0.017	254.1 ± 0.3	15.4 ± 0.5	176.40
0.018	254.1 ± 0.3	15.5 ± 0.5	204.08

As discussing above, light interference affects the fitted results. In order to eliminate the effect of light interference, the measured data in the vicinity of the $\frac{I_s}{I_{inc}}'$ s minimum was neglected. Thus Eq. 4 was used to fit the experimental data in the whole scattering vector range again. The fitted values are shown in Table 4.3. The values can be thought to be consistent with the fitted results obtained by using Eq. 1 in the fitting range with the small values of the scattering vector

Table 4.3 The fitted results of the sample *PNIPAM*–1 were obtained by using Eq. 4 and neglecting some experimental data.

b	$R_s(nm)$	$\sigma(nm)$	χ^2
0.013	251.3 ± 0.6	22.17 ± 0.05	79.80
0.014	251.1 ± 0.6	23.3 ± 0.9	58.29
0.015	250.9 ± 0.6	24.4 ± 0.8	44.50
0.016	250.7 ± 0.5	25.4 ± 0.7	37.02
0.017	250.5 ± 0.6	26.4 ± 0.7	36.01
0.018	250.3 ± 0.6	27.24 ± 0.8	41.59

Because $0.45 \mu m$ filters were used to do dust free for our samples, we can think that the very big particles do not exist. So the expected values calculated by using Eq. 4 and the fitted results obtained by using Eq. 1 in the fitting range with the small values of the scattering vector should be consistent with the experimental data if the number distribution has been corrected. The expected values calculated in three different situations for the sample *PNIPAM* – 1 are shown in Figure 4.2. The expected results in third situation are consistent with the experimental data.

For the particles of small sizes, the fitted results are shown in Table 4.4. The sample is *PNIPAM* – 5. The data was measured at temperature $40^\circ C$. The fitted results during the scattering vector range $0.00345 nm^{-1}$ to $0.02555 nm^{-1}$ are chosen as the size information obtained by using the SLS technique. Figure 4.3 shows the fitted results and the residuals during the scattering vector range $0.00345 nm^{-1}$ to $0.02555 nm^{-1}$.

Table 4.4 The fitted results of the sample *PNIPAM*–5 at different scattering vector ranges and T=40°C.

q (10 ⁻³ nm ⁻¹)	R_s (nm)	σ (nm)	χ^2
3.45 to 14.21	143.78±8.34	7.32±14.78	2.68
3.45 to 16.10	116.70±7.35	27.01±3.40	2.97
3.45 to 17.87	130.01±3.54	19.45±2.41	2.92
3.45 to 19.50	142.29±2.33	7.26±4.48	4.43
3.45 to 20.98	138.18±1.50	13.47±1.57	3.97
3.45 to 23.46	142.30±0.57	7.97±1.22	3.18
3.45 to 24.44	140.09±0.46	11.59±0.73	3.66
3.45 to 25.23	139.57±0.41	12.33±0.63	3.87
3.45 to 25.55	139.34±0.31	12.36±0.55	5.50

For the sample *PNIPAM*–5, due to the values of qR_s are small, so the Zimm plot can be used to obtain the approximative value of the root mean square radius of gyration $\langle R_g^2 \rangle^{1/2}$. The results of the Zimm plot is shown in Figure 4.4. The value of $\langle R_g^2 \rangle^{1/2}$ is about 115.55 nm.

4.2 Simulative Data Analysis

In order to conveniently discuss the effects of the reflective light and the noises, the simulative data has been produced with the Gaussian distribution.

4.2.1 Simulative data of large particles

For large particles, both the effects of the reflective light and the noise must be considered. First, the effect of the reflective light is considered. The simulative data of the incident light was produced by using Eq. 1 and the data of the reflective light was obtained by using the following equation

$$\frac{I_s}{I_{inc}} = a \frac{4\pi\rho}{3} \frac{b \int_0^\infty R_s^6 P(q', R_s) G(R_s) dR_s}{\int_0^\infty R_s^3 G(R_s) dR_s}. \quad (11)$$

Then the 1% statistical noise was added to the simulative data respectively. Next we will keep the simulative data and only consider the effect of the reflective light.

The scattered intensity of the reflective light was added to the total scattered intensities. When the final data of $\frac{I_s}{I_{inc}}$ was obtained, the 3% random errors were added. The simulative data 1 was produced when the mean radius was set 267 nm and the standard deviation was 23 nm. The fitted results by using Eq. 1 at different scattering vector ranges are listed in Table 4.5 for the value of b was chosen to be 0.015. The results show that the fitted result's errors decrease and the mean radius and the standard deviation approximate constant values when the fitting scattering vector range is enlarged. Figure 4.5 shows the fitted results and the residuals during the scattering vector range 0.00345 nm⁻¹ to 0.01592 nm⁻¹.

Table 4.5 The fitted results of the simulative data 1 with $b=0.015$ at different scattering vector ranges.

$q (10^{-3} nm^{-1})$	$\bar{R}_s(nm)$	$\sigma(nm)$	χ^2
3.45 to 10.97	272.52 ± 1.76	12.97 ± 4.56	0.81
3.45 to 12.01	271.18 ± 1.06	16.00 ± 2.30	0.75
3.45 to 13.02	269.41 ± 0.68	19.40 ± 1.25	0.76
3.45 to 14.02	267.45 ± 0.22	22.64 ± 0.42	0.82
3.45 to 14.98	266.95 ± 0.03	23.53 ± 0.17	0.88
3.45 to 15.92	266.96 ± 0.02	23.45 ± 0.09	0.82

Since the Gaussian distribution was used to produce the simulative data, so Eq. 4 can be used to fit the data at the whole scattering vector range. The fitted results with the different values of b are listed in Table 4.6. The fitted results are consistent with those obtained by using Eq. 1 in the fitting range with the small values of the scattering vector.

Table 4.6 The fitted results of the simulative data 1 with $b=0.015$ were obtained by using Eq. 4.

b	$\bar{R}_s(nm)$	$\sigma(nm)$	χ^2
0.012	266.62 ± 0.22	22.80 ± 0.24	28.06
0.013	266.67 ± 0.15	22.91 ± 0.17	13.64
0.014	266.72 ± 0.09	23.01 ± 0.098	4.73
0.015	266.758 ± 0.001	23.14 ± 0.03	1.00
0.016	266.83 ± 0.07	23.22 ± 0.08	2.76
0.017	266.89 ± 0.13	23.32 ± 0.14	9.39
0.018	266.95 ± 0.198	23.43 ± 0.21	20.87

The fitted results obtained by using Eq. 1 in the scattering vector range $0.00345 nm^{-1}$ to $0.01592 nm^{-1}$ were input Eq. 1 and Eq. 4 to calculate the expected values at the whole scattering vector range with b : 0.015, respectively. The results are shown in Figure 4.6. The expected results are consistent with the simulative data.

In order to investigate the effect of the reflective light on the fitted results obtained by using Eq. 1 in a fitting range with the small values of the scattering vector. The simulative data was produced for $b=0.0$, 0.005, 0.01 and 0.02 respectively. The fitted results at the same scattering vector range $0.00345 nm^{-1}$ to $0.01592 nm^{-1}$ are listed in Table 4.7. The fitted values show that the size information can be accurately obtained by using Eq. 1 in the fitting range with the small values of the scattering vector and the effect of the reflective light do not need to be considered.

Table 4.7 The fitted results of the simulative data 1 with the different reflective light.

b	$\bar{R}_s(nm)$	$\sigma(nm)$	χ^2
0	267.15 ± 0.02	23.103 ± 0.09	0.84
0.005	267.08 ± 0.02	23.22 ± 0.09	0.82
0.01	267.01 ± 0.02	23.42 ± 0.13	0.83
0.015	266.96 ± 0.02	23.45 ± 0.09	0.82
0.020	266.89 ± 0.02	23.56 ± 0.09	0.83

Second, the effect of noises will be considered. The fitted results of simulative data 1 with different noises and the different values of b at the scattering vector range 0.00345 nm^{-1} to 0.01592 nm^{-1} are shown in Table 4.8. The results show that the noises do not affect the fitted values.

Table 4.8 The fitted results of the simulative data 1 with the different noises and reflective light.

	$R_s(\text{nm})$	$\sigma(\text{nm})$	χ^2
0	267.141 ± 0.001	23.09 ± 0.06	1.20
0.005	266.91 ± 0.07	23.2 ± 0.1	1.55
0.01	266.82 ± 0.03	23.30 ± 0.04	0.61
0.015	266.95 ± 0.03	23.736 ± 0.08	1.71
0.02	266.82 ± 0.04	23.6 ± 0.2	2.91

4.2.2 Simulative data of small particles

For small particles, only the effect of noises need to be considered. The simulative data 2 was produced when the mean radius was set 90 nm and the standard deviation was 7 nm . The final simulative data was obtained in two different situations: one is that the noise was not added (*first*) and the other is that the 1% statistical noise was added (second to fifth). The fitted results are listed in Table 4.9. The values show that the fitted results are affected by the noise. Figure 4.7 shows the fitted results and residuals of the fifth simulative data of the simulative data 2.

Table 4.9 The fitted results of the simulative data 2 with different noises.

	$R_s(\text{nm})$	$\sigma(\text{nm})$	χ^2
First	89.97 ± 0.08	7.02 ± 0.09	0.004
Second	87.2 ± 3.0	10.5 ± 2.5	1.41
Third	79.0 ± 3.4	15.4 ± 1.7	2.02
Fourth	77.5 ± 2.3	16.2 ± 1.2	0.84
Fifth	91.2 ± 1.2	4.9 ± 2.0	1.94

If the simulative data 2 with the different noises is put together, as shown in Figure 4.8, the difference among the simulative data 2 with the different noises can not be distinguished. From the Zimm plot analysis, the root mean square radius of gyration $\langle R_g^2 \rangle^{1/2}$ and the Zimm's molecular mass of particles will be same. However, due to the size distribution, the average molecular mass of particles $\langle M \rangle$ will have large differences for the particles with different distributions. Figure 4.9 shows the results by using the Zimm plot to fit the third simulative data of the simulative data 2. For the five simulative data, the fitted values of $\langle R_g^2 \rangle$ are listed in Table 4.10. If the symbol k is used to represent the quantity $M_z / \langle M \rangle$. The expected values of $\langle R_g^2 \rangle_{cal}^{1/2}$ and k obtained by using Eqs. 9 and 10 are also shown in Table 4.10.

Table 4.10 The experimental and expected values of $\langle R_g^2 \rangle^{1/2}$ and the values of k .

	$\langle R_g^2 \rangle^{1/2}$ (nm)	$\langle R_g^2 \rangle_{cal}^{1/2}$ (nm)	k
First	74.96	72.36	1.05
Second	75.46	73.46	1.13
Third	73.67	73.97	1.32
Fourth	73.12	74.17	1.36
Fifth	74.96	71.95	1.03

Due to the value of k has a strong dependence on the distribution of particles, the simulative data 3 was produced as the simulative data 2 with the mean static radius 50 nm and the standard deviation 10 nm. The fitted results are listed in Table 4.11. The fitted values of $\langle R_g^2 \rangle$ obtained by using Zimm plot and the expected values of $\langle R_g^2 \rangle_{cal}^{1/2}$ and k obtained by using Eqs. 9 and 10 are shown in Table 4.12.

Table 4.11 The fitted results of the simulative data 3 with different noises.

	R_s (nm)	σ (nm)	χ^2
First	50.5 ± 0.2	9.76 ± 0.08	9.9×10^{-5}
Second	57.3 ± 3.2	5.1 ± 3.0	0.46
Third	42.3 ± 5.4	12.5 ± 1.9	3.39
Fourth	58.7 ± 0.8	3.9 ± 0.9	0.30
Fifth	58.96 ± 0.01	3.6 ± 0.2	2.57

Table 4.12 The experimental and expected values of $\langle R_g^2 \rangle^{1/2}$ and the values of k .

	$\langle R_g^2 \rangle^{1/2}$ (nm)	$\langle R_g^2 \rangle_{cal}^{1/2}$ (nm)	k
First	48.41	47.17	1.31
Second	48.40	46.58	1.07
Third	47.72	46.36	1.67
Fourth	48.47	46.74	1.04
Fifth	46.34	46.75	1.03

5 Results and Discussion

From the analysis of simulative data, for the large particles the reflective light and the noises do not need to be considered when the size information is obtained from the SLS data in the fitting range with the small values of the scattering vector. We ever produced the simulative data for the wide distribution and much larger size. The conclusion is the same with that obtained from the simulative data 1. For the wide distribution, the mean radius 267 nm and the standard deviation 134 nm were used to produce the simulative data, the fitted results during the scattering vector range 0.00345 nm^{-1} to 0.01498 nm^{-1} : the mean radius is $267.5 \pm 0.9 \text{ nm}$, the standard deviation is $134.2 \pm 0.5 \text{ nm}$ and χ^2 is 0.91. The expected values calculated by inputting the results in Eq. 1 and 4 respectively are shown in Figure 5.1.

For the much larger size, the mean radius 500 nm and the standard deviation 15 nm were used to produce the simulative data, the fitted results during the

scattering vector range 0.00345 nm^{-1} to 0.00969 nm^{-1} : the mean radius is $500.10 \pm 0.04 \text{ nm}$, the standard deviation is $15.20 \pm 0.04 \text{ nm}$ and χ^2 is 0.37. The expected values calculated by inputting the results in Eq. 1 and 4 respectively are shown in Figure 5.2.

How to obtain the values of $\langle R_g^2 \rangle^{1/2}$ has been shown. The fitted results by choosing the different data points are listed in Table 5.1. The results show that the values almost keep constant for the different fitting ranges.

Table 5.1 The values of $\langle R_g^2 \rangle^{1/2}$ of the simulative data 2 with the different noises.

Fitted points	$\langle R_g^2 \rangle^{1/2} (\text{nm})$				
	First	Second	Third	Fourth	Fifth
1 to 15	74.46	70.60	73.16	74.62	78.19
1 to 20	74.96	75.50	73.67	73.13	74.96
1 to 25	75.62	76.26	75.99	75.12	74.65
1 to 30	76.43	77.58	77.46	77.73	75.64
1 to 35	77.28	77.76	77.61	78.07	76.48

For the experimental data measured from the real particles, the size information can be obtained by fitting the data in the range with the small values of the scattering vector as the size information of the sample *PNIPAM* – 1 at temperature 29°C was obtained. Due to the PNIPAM microgels possess the temperature sensitivity during the temperature rang $15^\circ\text{C} – 50^\circ\text{C}$, in order to show the phase transition of the different samples together, the static radii $R_s^{40^\circ\text{C}}$ of the four PNIPAM microgels at temperature 40°C are used as the standard values respectively, the ratios between the static radii R_s^T at temperature T and $R_s^{40^\circ\text{C}}$ are shown in Figure 5.3.

From the chemical knowledge, the materials of PNIPAM possess the temperature sensitivity. If adding the N, N' -methylenebisacrylamide, the temperature sensitivity of PNIPAM microgels will be affected by the content of the N, N' -methylenebisacrylamide which does not possess the temperature sensitivity. If the content of the N, N' -methylenebisacrylamide continues to increases, the temperature sensitivity of PNIPAM microgels is becoming disappearance. Figure 5.3 clearly shows the feature. The phase transition of PNIPAM microgels, indicated as the ratios $R_s^T/R_s^{40^\circ\text{C}}$ vs T , becomes less sharp and occurs in a broader T range as the N, N' -methylenebisacrylamide content increases.

Since the sizes of PNIPAM microgel particles at high temperature are small, the fitted values will be affected by the noises as we have discussed for the simulative data, but this method still can give the better values of $\langle R_g^2 \rangle^{1/2}$ as we have discussed and let us avoid the stringent requirements for the sample quality and the instrument at much smaller scattering angles. The fitted values of the four PNIPAM microgel samples at high temperatures are listed in Table 5.2. All the experimental data of the sample *PNIPAM* – 5 and the results obtained by using the Zimm plot in a range with the small values of the scattering vector are shown in Figure 5.4. The picture shows that the values of $\langle R_g^2 \rangle^{1/2}$ obtained by using the Zimm plot have a large uncertainty. The value is decided by the fitted

data. Even if the data points that apparently deviate from the linear range were neglected, the values of $\langle R_g^2 \rangle^{1/2}$ still show strong dependence on the fitted points. For the four PNIPAM microgel samples, the fitted results are shown in Table 5.3.

Table 5.2 The fitted results of the four PNIPAM microgel samples at high temperatures.

Sample(Temperature)	R_s (nm)	σ (nm)	χ^2
<i>PNIPAM</i> – 5 (40°)	139.3±0.3	12.4±0.6	5.50
<i>PNIPAM</i> – 2 (40°)	114.4±0.9	11.4±1.1	4.34
<i>PNIPAM</i> – 1 (40°)	111.7±0.9	14.8±0.8	2.73
<i>PNIPAM</i> – 0 (40°)	101.7±1.1	8.6±1.3	1.80
<i>PNIPAM</i> – 0 (34°)	93.4±1.9	24.5±0.9	1.56

The fitted values of the experimental data of the four PNIPAM microgel samples measured at high temperatures were input to Eqs. 9 and 10 respectively to obtain the expected values of $\langle R_g^2 \rangle_{cal}^{1/2}$ and k . The values are listed in Table 5.3.

Table 5.3 The experimental and expected values of $\langle R_g^2 \rangle^{1/2}$ and the values of k .

Sample(Temperature)	$\langle R_g^2 \rangle_{cal}^{1/2}$ (nm)	$\langle R_g^2 \rangle^{1/2}$ (nm)	k
<i>PNIPAM</i> – 5 (40°)	113.23	113.73 to 122.85	1.07
<i>PNIPAM</i> – 2 (40°)	94.05	89.39 to 125.89	1.09
<i>PNIPAM</i> – 1 (40°)	95.58	88.62 to 164.87	1.15
<i>PNIPAM</i> – 0 (40°)	82.28	74.78 to 86.36	1.06
<i>PNIPAM</i> – 0 (34°)	97.15	102.48 to 113.06	1.55

6 Conclusion

The consistency between the theoretical results and static light scattering data shows that the size information can be obtained by using the non-linear least squares fitting method and the SLS data in this form $I(q) vs q$ contain sensitive size information of particles. For the large particles, the reflective light and the noises do not affected the fitted results in the range with the small values of the scattering vector and the accurate size information can be obtained.

For small size particles, although the fitted values are affected by the noises, this still is a good method to obtain the size information from the SLS data. It can give a better approximative value of $\langle R_g^2 \rangle^{1/2}$ and avoid the stringent dependence on the sample quantity and the instrument. The molecular mass of particles measured by using the Zimm plot is a better approximative value of the average molecular mass of particles only for the particle systems with very narrow distributions.

The simple number distribution $G(R_s)$ obtained from the SLS data is the distribution that people really want to obtain from the experimental data. The simple number distribution $G(R_s)$ can let us only consider the effects of the parameter size and avoid the effects of other parameters when we analyze other physical quantities.

Fig. 4.1 The experimental and fitted results of the sample *PNIPAM* – 1 at temperature $29^{\circ}C$. The circles show the experimental data, the line shows the fitted results and the diamonds show the residuals= $(y_i - y_{fit}) / \sigma_i$.

Fig. 4.2 The experimental and expected results of the sample *PNIPAM* – 1. The circles show the experimental data, the line shows the expected results of the incident light calculated during the whole particle size distribution range, the stars show the expected results of the incident light calculated between about the $\bar{R}_s - 1.3\sigma$ and $\bar{R}_s + 1.3\sigma$ and the diamonds show the expected results of the incident and the reflective light calculated between about the $\bar{R}_s - 1.3\sigma$ and $\bar{R}_s + 1.3\sigma$ with b: 0.014.

Fig. 4.3 The experimental and fitted results of the sample *PNIPAM* – 5 at temperature $40^{\circ}C$. The circles show the experimental data, the line shows the fitted results and the diamonds show the residuals= $(y_i - y_{fit}) / \sigma_i$.

Fig. 4.4 The Zimm plot of the sample *PNIPAM* – 5 at temperature $40^{\circ}C$. The circles show the experimental data and the line shows a linear fit to the plot of KC/R vs q^2 .

Fig. 4.5 The experimental and fitted results of the simulative data 1 with b=0.015. The circles show the experimental data, the line shows the fitted results and the diamonds show the residuals= $(y_i - y_{fit}) / \sigma_i$.

Fig. 4.6 The experimental and expected results of the simulative data 1 with b=0.015. The circles show the experimental data, the line shows the expected results of the incident light calculated during the whole particle size distribution range and the diamonds show the expected results of the incident and reflective light calculated during the whole particle size distribution range with b: 0.015.

Fig. 4.7 The experimental and fitted results of the fifth simulative data of the simulative data 2. The circles show the experimental data, the line shows the fitted results and the diamonds show the residuals= $(y_i - y_{fit}) / \sigma_i$.

Fig. 4.8 The simulative data 2 with the different noises.

Fig. 4.9 The Zimm plot of the third simulative data of the simulative data 2. The circles show the simulative data and the line shows a linear fit to the plot of I_{inc}/I_s vs q^2 .

Fig. 5.1 The experimental and expected results of the simulative data. The circles show the experimental data, the line shows the expected results of the incident light calculated during the whole particle size distribution range and the diamonds show the expected results of the incident and reflective light calculated during the whole particle size distribution range with b: 0.01.

Fig. 5.2 The experimental and expected results of the simulative data. The circles show the experimental data, the line shows the expected results of the incident light calculated during the whole particle size distribution range and the diamonds show the expected results of the incident and reflective light calculated during the whole particle size distribution range with b: 0.01.

Fig. 5.3 The ratios of the static radii $R_s^T / R_s^{40^{\circ}C}$ of the samples *PNIPAM* – 0, *PNIPAM* – 1, *PNIPAM* – 2 and *PNIPAM* – 5 at different temperatures.

Fig. 5.4 The results of the Zimm plot and the experimental data of the sample *PNIPAM* – 5 at temperature $40^{\circ}C$ in a large scattering vector range.

The circles show the experimental data and the line shows the results of Zimm plot obtained in a range with the small values of the scattering vector.

- [1] P. N. Pusey and W. van Megen, *J. Chem. Phys.*, 1984, 80, 3513
- [2] K. B. Strawbridge and F. R. Hallett, *Macromolecules*, 1994, 27, 2283
- [3] H. Schnablegger and O. Glatter, *J. Colloid. Interface Sci.* 1993, 158, 228
- [4] B. H. Zimm, *J. Chem. Phys.* 1948, 16, 1099
- [5] W. Burchard, *Adv. Polym. Sci.* 1983, 48, 1
- [6] B. Chu, *Laser Light Scattering: Basic Principles and Practice*, Academic Press, Inc. New York, 1991
- [7] J. Gao and B. J. Frisken, *Langmuir*, 2003, 19, 5217
- [8] J. Gao and B. J. Frisken, *Langmuir*, 2003, 19, 5212

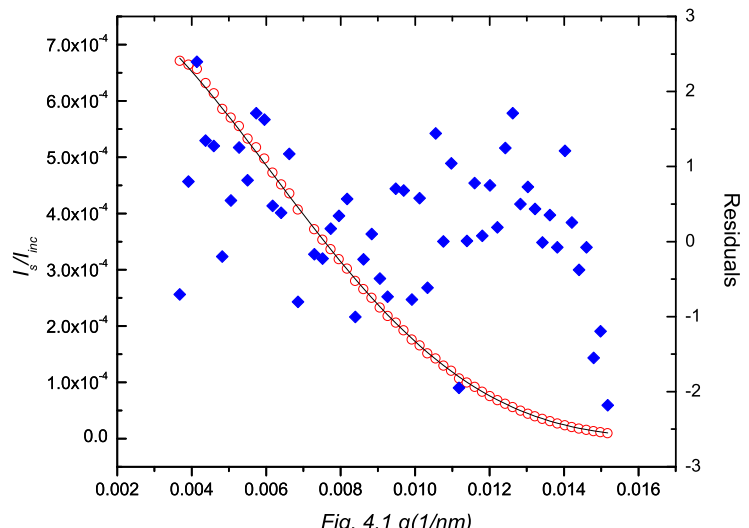


Fig. 4.1 q (1/nm)

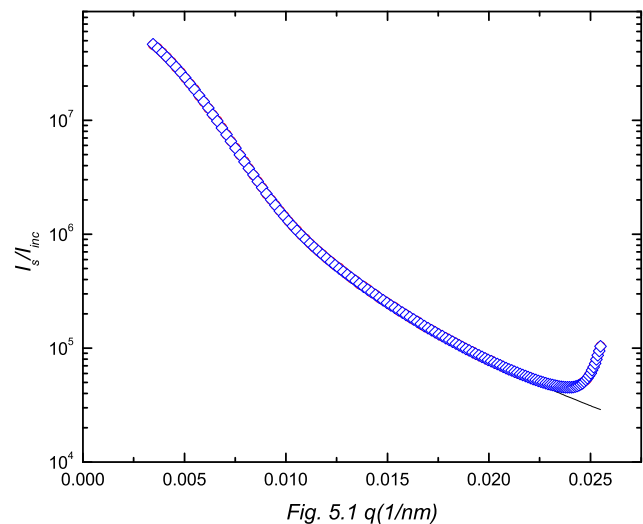


Fig. 5.1 $q(1/\text{nm})$

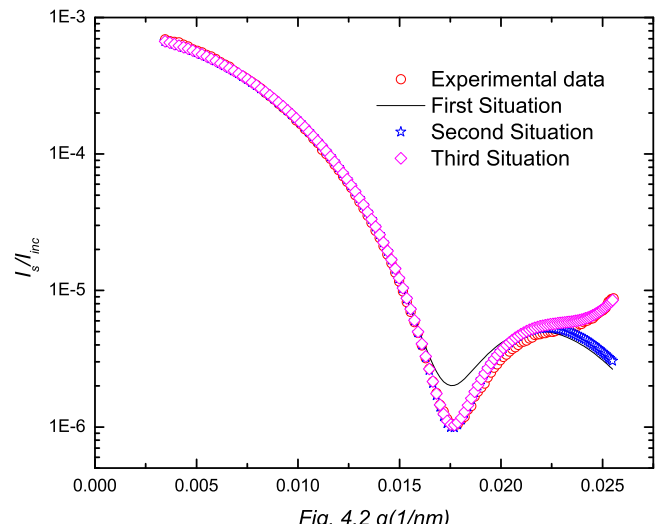


Fig. 4.2 $q(1/\text{nm})$

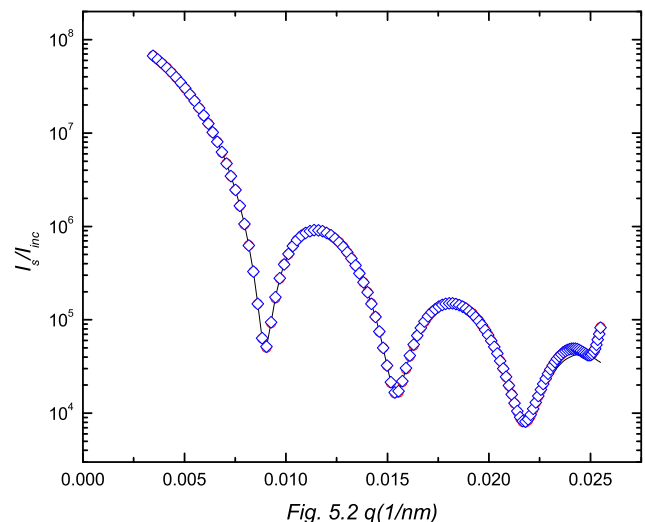


Fig. 5.2 $q(1/\text{nm})$

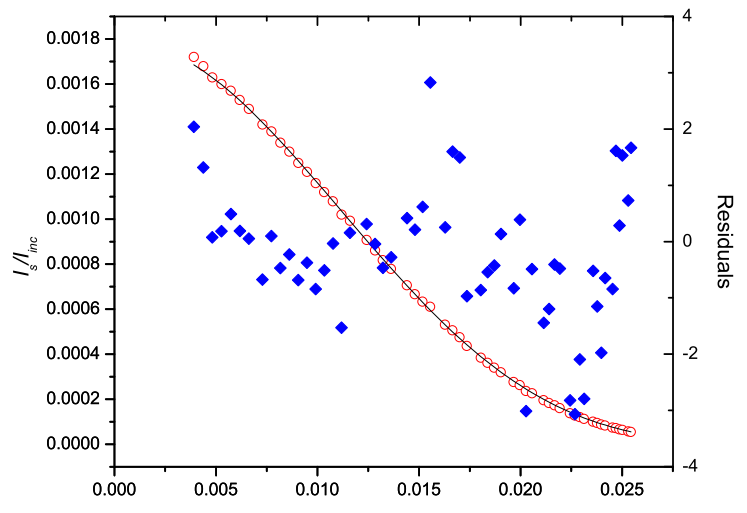


Fig. 4.3 q (1/nm)

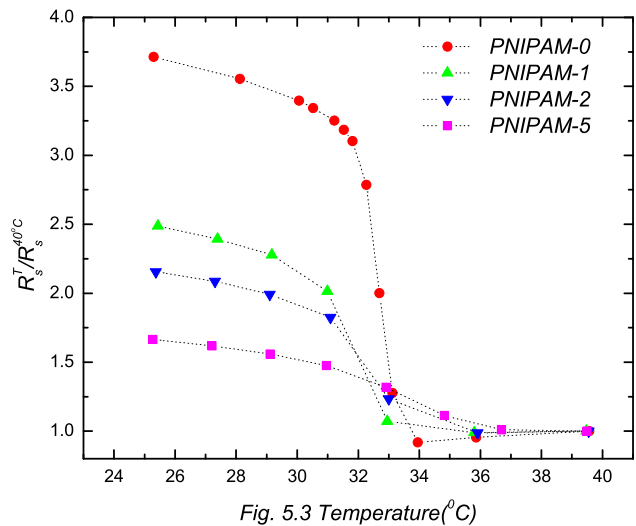


Fig. 5.3 Temperature ($^{\circ}\text{C}$)

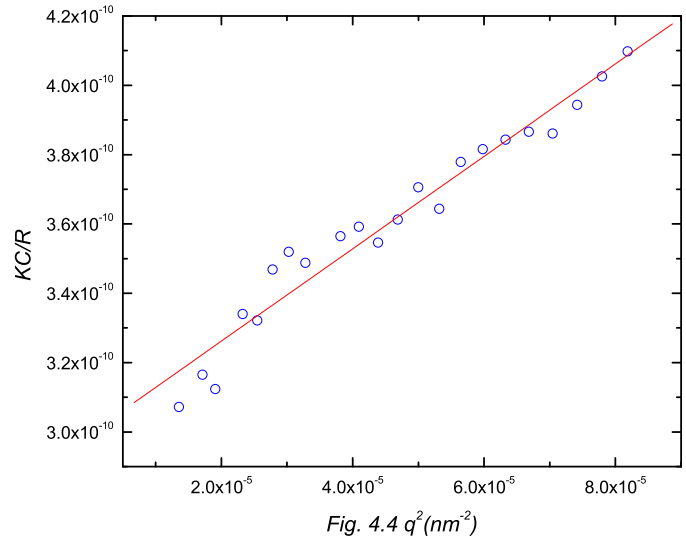


Fig. 4.4 q^2 (nm⁻²)

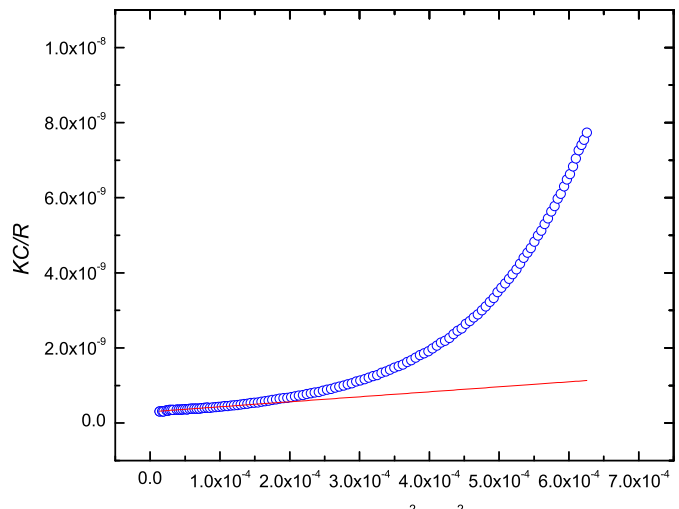


Fig. 5.4 q^2 (nm⁻²)

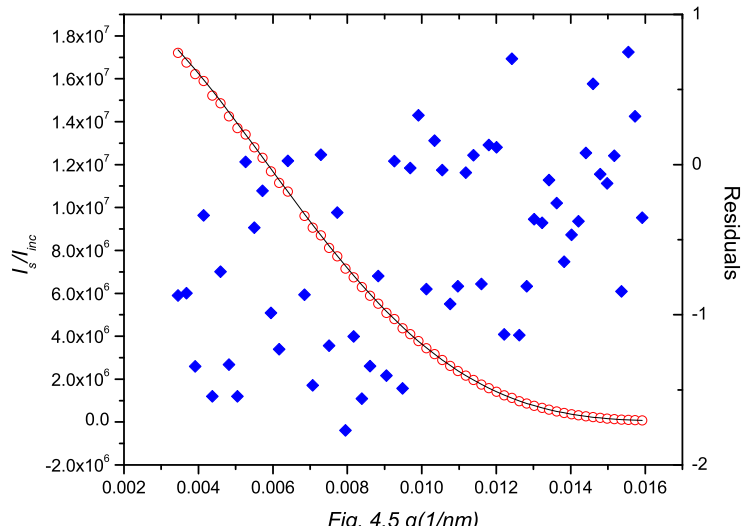


Fig. 4.5 $q(1/\text{nm})$

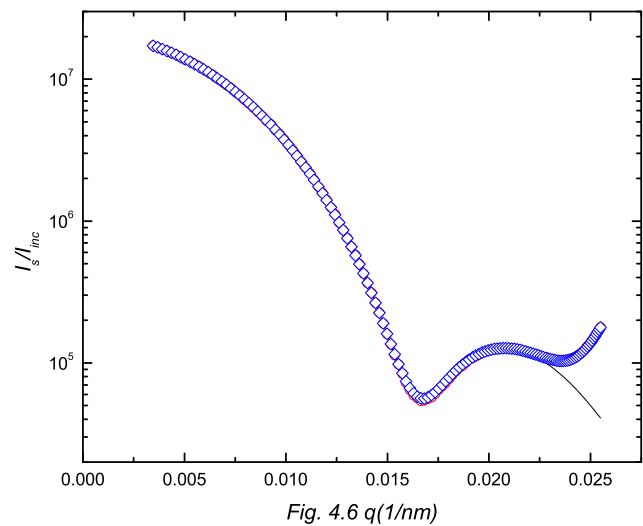


Fig. 4.6 $q(1/\text{nm})$

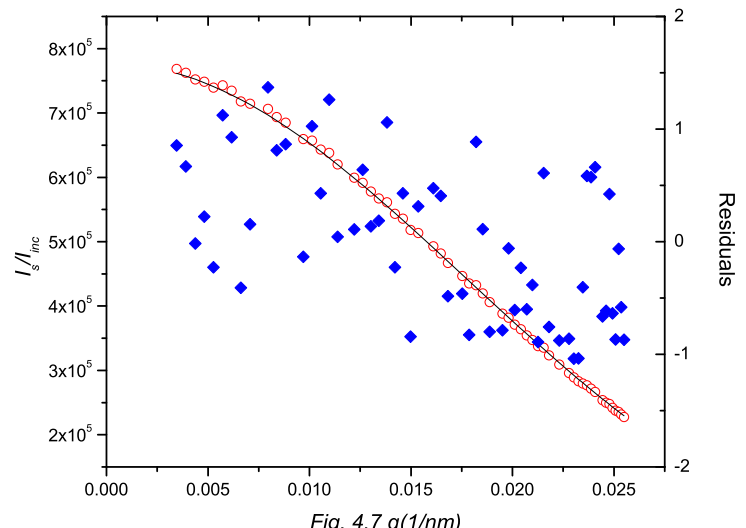


Fig. 4.7 q (1/nm)

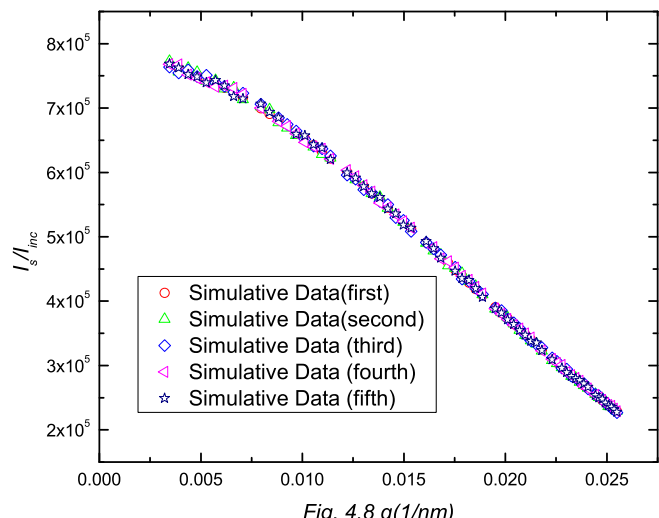


Fig. 4.8 q (1/nm)

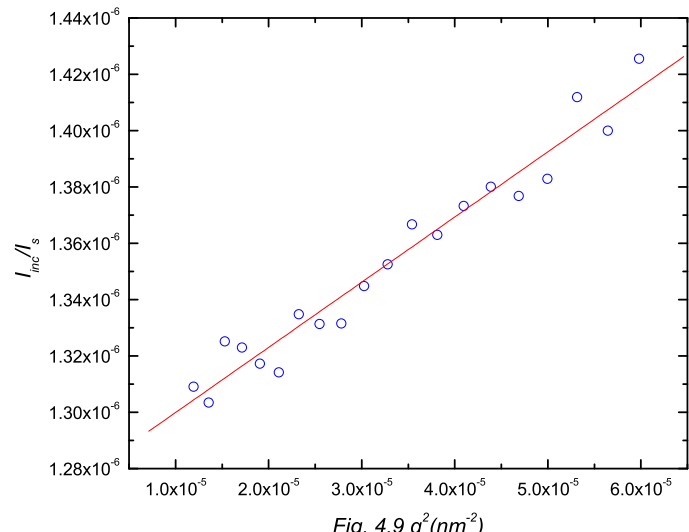


Fig. 4.9 $q^2 (nm^{-2})$